Construction and Building Materials 298 (2021) 123851

Contents lists available at ScienceDirect

Construction and Building Materials

journal homepage: www.elsevier.com/locate/conbuildmat

Dropwise condensation freezing and frosting on bituminous surfaces at subzero temperatures

F. Tarpoudi Baheri [a,b], L.D. Poulikakos [b], D. Poulikakos [a,*], T.M. Schutzius [a,1]

[a] Laboratory of Thermodynamics in Emerging Technologies, Department of Mechanical and Process Engineering, ETH Zurich, Sonneggstrasse 3, CH-8092 Zurich, Switzerland
[b] Laboratory for Concrete and Asphalt, Empa, Ueberlandstrasse 129, CH-8600 Duebendorf, Switzerland

HIGHLIGHTS

- PCM microcapsule modification can delay frosting on bitumen in repeatable cycles.
- Condensation deposit forms around freezing droplet while its temperature jumps 0°C.
- Bitumen temperature and *RH* controls initial condensation regardless of cooling rate.
- Water freezes on bitumen at lower temperatures at low *RH* or fast cooling rates.
- Cascade freezing expands across supercooled droplets, ice bridging links droplets.

GRAPHICAL ABSTRACT

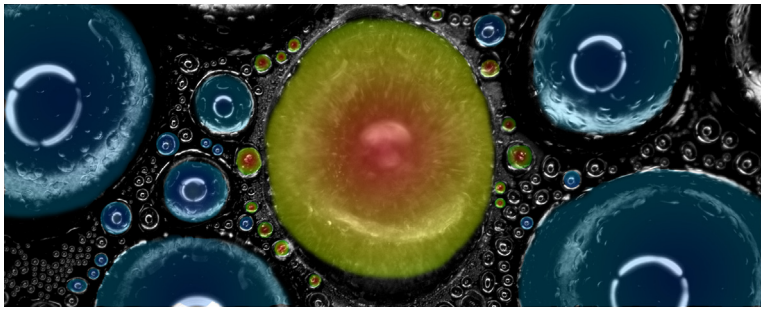

ARTICLE INFO

Article history:
Received 13 November 2020
Received in revised form 11 March 2021
Accepted 1 June 2021

Keywords:
Bitumen
Phase change materials
Condcondensation freezing
Icephobicity
Icing
Frosting
Modified winter asphalt binder
Freezing delay

ABSTRACT

Freezing of atmospheric water on bituminous construction and road surfaces is a recurring event during winter. However, droplet freezing on bitumen and passive inhibition methods are poorly understood. Here we investigate relative humidity and substrate cooling effects on condensation freezing on subzero temperature bituminous surfaces and find that droplet freezing is explosive, with rapid local heating. We explain the related physics and find that relative humidity and cooling rate can affect droplet sizes and freezing temperatures. We then rationally embed phase change material microcapsules in bitumen, harnessing their latent heat to significantly delay freezing, demonstrating a viable option for frost mitigation.

1. Introduction

In countries with severe winter weather conditions, the clearance and maintenance of roads, roofs, and runways in winter is essential to ensure safe driving, living, and transportation conditions. Roads and many construction surfaces are commonly bitumen-based, and roads usually contain ca. 5 wt% of bitumen (less than 20% by volume fraction) [1]. Despite its low percentage,

* Corresponding author at: ETH Zurich, Laboratory of Thermodynamics in Emerging Technologies, Sonneggstrasse 3, ML J 36, CH-8092 Zurich, Switzerland.
E-mail addresses: dpoulikakos@ethz.ch (D. Poulikakos), thomschu@ethz.ch (T.M. Schutzius).
[1] Present Address: ETH Zurich, Laboratory for Multiphase Thermofluidics and Surface Nanoengineering, Sonneggstrasse 3, ML J 27.2, CH-8092 Zurich, Switzerland.

https://doi.org/10.1016/j.conbuildmat.2021.123851
0950-0618/

bitumen is the costliest portion of the mixture and due to its role as a binder and coating of aggregates, it has an important role on the overall mechanical and surface chemistry properties. Ice accumulation on bitumen-based surfaces, and in particular roads, is a multimillion-dollar problem with hidden costs such as asphalt road degradation (especially bitumen), and it has strategic and economic ramifications and drawbacks ranging from delays in the delivery of goods to an increase in vehicular fuel consumption [2,3]. Furthermore, several studies have shown a connection between road accidents and weather and pavement conditions in winter [4–8].

To address this problem, winter maintenance methods are employed, which can be categorized into two groups: passive methods (i.e., real-time maintenance is not needed) and active methods (i.e., site operation is needed). Conventional winter maintenance methods are mostly limited to active methods, which include chemical deicers, brine, and salt (predominantly sodium chloride). Salt is used to melt snow and ice, and is most effective at temperatures above − 11 °C, close to the melting temperature of ice [8,9]. The methods mentioned above may seem attractive at first, according to their low initial capital costs and facility of use [10], but eventually, salt and chemical deicers result in pavement degradation, which shortens the pavement service life [11,12] and can be harmful to the environment, for example through freshwater salting [13]. Therefore, it is necessary to first improve our fundamental understanding of freezing on bituminous surfaces at the microscopic level, starting with dropwise frost formation from the condensation of environmental vapor, and then seek alternative, preferably passive methods for its deterrence. To this end, a possible passive method of mitigating the day and night temperature gradient leading to water freezing on bituminous surfaces, is to use phase change materials (PCM) in the bitumen composition, which act as thermal capacitors. It has been shown that temperature variations of PCM modified asphalt, caused by the daily temperature cycle, can be adjusted with the help of the latent heat of fusion of PCM [14].

Here we investigate the effect of environmental and surface temperature, relative humidity, and substrate cooling rates on condensation and ice formation and propagation on the surface of bitumen using optical microscopy and infrared imaging techniques in a controlled climate chamber. Our results show that the initial condensation temperature is sensitive to the environmental relative humidity percentage (*RH%*); however, it is practically independent of the cooling rate. After condensation, supercooled (an unstable state of a liquid below its freezing point) droplets can remain in the liquid state at lower subzero temperatures when, being cooled at faster rates or are in lower relative humidity conditions, where the droplets have smaller volumes. We then studied the physics of the ensuing explosively rapid freezing process from the supercooled water state and also capture and discuss an interesting mechanism of natural ice bridging among freezing drops, leading to frost propagation on a bituminous surface. Finally, we select and embed a phase change material (PCM) in the bitumen, at high-enough concentrations that still do not significantly affect mechanical [15] or surface properties, and study its heating effect upon solidification in delaying frosting, using differential scanning calorimetry and infrared imaging. We show that by rationally embedding PCMs within bitumen, we can markedly suppress and delay surface icing.

2. Materials and methods

2.1. Materials

This study was conducted on virgin bitumen Q8 70/100 (penetration grade 70/100, density 1.029 g/cm^3, of Middle Eastern origin) with a medium softness range of 82 (0.1 mm) needle penetration (EN 1426) and softening temperature (EN 1427) of 45.8 °C and dynamic viscosity of 163 Pa-s at 60 °C. For this type of bitumen, differential scanning calorimetry (DSC) results show a glass transition temperature of ca. −20 °C and a melting peak of ca. 28 °C with reported SARA (saturates, aromatics, resins, and asphaltene) factions of 3.8, 59.6, 22.2 and 14.6%, respectively [16,17].

Direct tetradecane (a liquid PCM chemical) additives to bitumen target the principal properties of bitumen, which are critical for its performance in asphalt concrete [18]. Unlike the direct addition of such a PCM chemical, which softens the original bitumen and affects its principal properties [18], microencapsulated PCM can survive the high temperatures and pressure that bitumen is exposed to during the artificial aging process without compromising its properties. It has also been experimentally shown that microencapsulated PCM safeguards bitumen from cold temperature cracks by releasing heat and improves bitumen's mechanical performance in subzero conditions [19]. PCM microcapsules can affect the mechanical properties of the modified bitumen although previous work has shown that PCM microcapsules at 25 wt% concentration in bitumen does not negatively impact the mechanical properties of the bitumen binder at cold temperatures [15]. When latent heat is released by PCM microcapsules during crystallization, this can lead to bitumen softening at cold temperatures. Once crystallized, the PCM microcapsules can increase the complex modulus of bitumen, similar to filler minerals [15]. Concerning the leakage of the microcapsules, the PCM wax could potentially function as a rejuvenator oil for aged bitumen [15]. Microencapsulated PCM particles can be added during different stages of asphalt concrete preparation, and it has been reported that both wet (added to bitumen) and dry (added to asphalt mixture) processes alike have resulted in improved performance compared to non-modified reference samples [20].

We selected a microcapsule PCM (μPCM-21) fabricated by Microtek Labs, USA, to modify the bitumen in order to investigate icing delay. The core of the microcapsules consists of tetradecane (n-alkane $C_{14}H_{30}$), which has a melting temperature of ~ 6 °C and is known as a low-temperature phase change material [15]. Its average particle size is reported by Kakar et. al. [15,20] as being 21 μm with 0.834 g/cm^3 density and 195.5 J/g heat of fusion. The PCM material is encapsulated by a polymeric shell made of melamine–formaldehyde [15].

2.2. Solution preparation and coating

As a first step, the virgin bitumen was melted at 137 °C (mixing temperature) in an oven for 30 min. Then, the prepared dried microcapsules (at 110 °C for 5 min) were added to the melted virgin bitumen to reach 25% concentration by weight of the final blend. (Figure S1 and Supporting Information, section "A.1" illustrate the resistance of the PCM microcapsules to chemical, mechanical, and thermal stresses that they are exposed to during sample preparation.) Each of the virgin and modified melted bitumen solutions were then mixed in a speed mixer (Speed Mixer™, DAC 150.1 FVZ, Germany) for 2 min at 2,000 rpm. Next, 1 g of bitumen (virgin or PCM microcapsule modified) was removed with a spatula, and diluted in 4 ml toluene at 25 °C (Sigma-Aldrich 99.8%), then the entire solution was mixed using a shaker (Heidolph Multi Reax) at 2,000 rpm for 2 min. (Figure S2 in Supporting Information, section "A.2", shows a schematic drawing of the steps undertaken for the preparation of the sample.)

To fabricate thin virgin bitumen coatings, (termed "thin" virgin bitumen samples), we used a solvent casting approach. Here, 150 μl of the virgin bitumen solution was dispensed on a 22 mm diameter circular glass coverslip (Figure S2). The liquid drop cast

sample was left under a fume hood in ambient conditions until most of the toluene solvent evaporated, which we observed to occur within half an hour. Next, the samples were heated on a hotplate at 115 °C for 5 min, which is above the bitumen softening temperature and the toluene boiling temperature at 111 °C, to ensure uniform and smooth surfaces. Thereafter, the samples were placed in a refrigerator for 5 min at 4 ± 2 °C to cool and solidify the bitumen layer on glass coverslips. Based on the mass and geometry of the sample and density of bitumen, the final bitumen thickness is expected to be ≈100 μm. This was further measured using an optical microscope (see Supporting Information, section "A.2" and Figure S3). This sample preparation method produces a smooth bitumen surface. We note that it is different from real-world conditions, where the surface of bitumen can be contaminated by foreign substances. Such idealized surfaces are useful for gaining fundamental insight into the effect of bitumen alone on ice formation.

To highlight the PCM effect, thicker bitumen samples (termed "thick" bitumen samples) were cast using layer by layer drop-casting technique to obtain a ~ 1 mm sample thickness as explained above for the thin films. Such samples were fabricated in Petri dishes, which had a diameter of 29 mm and a height of 10 mm. The final sample comprised four layers, with each layer originally containing 1,000 μl of virgin or PCM-modified solution. After the application of each layer, the sample was heated to 115 °C for 5 min to evaporate the solvent. After the fourth layer, the Petri dish samples were cooled in a refrigerator (4 ± 2 °C) for 5 min. To ensure that the solvent evaporated, the samples were given approximately 24 h of conditioning time at room temperature before the experiments were conducted.

2.3. Experimental setup: Constant cooling rate

"Constant cooling rate" experiments were used to study how ice formed on the thin virgin bitumen samples. The designed sample holder controlled the sample temperature by means of a central ~ 1 mm diameter copper pin section installed on a Linkam BSC 196 cryogenic stage (Fig. 1a, Figure S4a, Supporting Information, section "A.3"). The probability of ice nucleation is much higher at colder temperatures [21]. Therefore, to ensure that we can observe the first droplet freeze, we opted to cool a limited region that we could visualize completely. Here, the sample should have a somewhat lower temperature relative to its surroundings, which also helps avoid the sample edge, which can affect condensation. The copper pin guarantees the initial condensation location, and freezing nucleation occurs in the field of view. Fig. 1a shows a schematic drawing of the experimental setup with the location of the copper pin, which was used to locally cool the thin bitumen samples from the center of the region of study. The red and green circular symbols show the location of the cryogenic stage temperature (T_2) and the copper temperature sensor (T_1), respectively. To control humidity, nitrogen gas flow passes through the water bubbler, and humidified nitrogen mixes with the bypassed nitrogen line to regulate the relative humidity (RH) of the outlet via flow control valves. The use of a clean and controlled environment prevents the surface of bitumen from being contaminated by dust and foreign particles. Such particles can promote both condensation freezing nucleation and increase the complexity of the process on bituminous surfaces. Condensation freezing experiments were performed at five experimental conditions consisting of three cooling rates of 1 °C/min, 10 °C/min, and 20 °C/min at RH 50% and three RH conditions of 20%, 50%, and 80% at 10 °C/min. The cryogenic stage operates at constant cooling based on the temperature feedback loop from T_2 (stage temperature). All experiments were initiated from T_2 = 25 °C after stabilization of the environmental temperature (T_{env} = 21.5 ± 0.5 °C) and the defined RH condition (20%, 50% or 80%), this setting remained untouched until the end of the defined constant cooling rate at T_2 = -50 °C, considering 2 min of conditioning time at T_2 = -50 °C. Over the course of the experiment we also continuously recorded RH, T_{env}, T_1 and image frames (at constant frame per second rate); later we also synchronized frames with T_2. We note that the maximum temperature difference between T_1 (copper pin) and T_2 (stage temperature) in all cases was less than 0.5 °C. Fig. 1b, c are images of the copper pin from the optical microscope and infrared (IR) cameras.

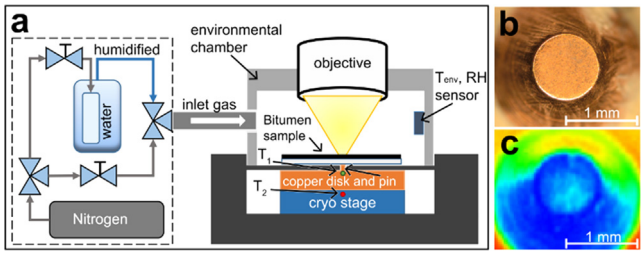

Fig. 1. Experimental setup for constant cooling rate. a) Condensation freezing setup. Schematic of the inlet nitrogen gas supply system in the dashed line box (not to scale). The location of the thermocouple in the copper stage, T_1, and the cryogenic stage feedback cryogenic stage, T_2, temperature sensors are shown as green and red dots, respectively. The environmental sensor records chamber environment temperature T_{env} and relative humidity percentage RH. The location of the optical microscope objective or IR camera lens is shown as "objective". b) Copper pin under the optical microscope at 5X magnification (without sample) and c) the same copper pin shown as seen from the IR camera (without sample). (For interpretation of the references to colour in this figure legend, the reader is referred to the web version of this article.)

The reported "condensation temperatures" were extracted from the corresponding frames of optical microscopy at the moment of detection of the first condensed droplets on the dry virgin bitumen surface (approximate resolution of 1 μm/pixel). We only recorded freezing events when supercooled droplets froze within the field of view, and the temperature of the corresponding frame is defined as the "freezing temperature". Optical microscopy was performed using an Olympus BX60 optical microscope at 5X magnification and constant illumination in dark field mode for the condensation freezing experiment and 100X magnification in bright field mode to capture ice bridging. In a separate equivalent cryogenic stage configuration and experiment conditions, a FLIR SC7000 infrared camera was used to study the condensation freezing. (The location of the optical microscope objective or IR camera lens is shown as "objective" in Figure S4a.)

2.4. Experiment setup: Constant cooling flux

The aim of the "constant cooling flux" experiments was to study ice formation on bitumen samples containing PCM. This was due to the fact that during constant cooling rate experiments, the feedback correction loop would compensate the heat released by the PCM. The constant cooling flux provides similar conditions without the existence of any correcting temperature feedback loop, thus capturing the heat released by the PCM microcapsules. We operated the thermoelectric element at constant input power, while the hot side of the thermoelectric element was kept at a constant temperature to reach stable constant cooling flux conditions on the cold side [22] (Figure S4b). To do this, another large temperature stage (CP-200HT-TT device from TE Technology Inc.) was used to keep the hot side of the thermoelectric element at 0 °C (see Figure S4b in Supporting Information, section "A.3"). At the given conditions, a thermoelectric element from Laird technologies™ (PC6-12-F1-4040-TA-W6) operated with constant 5 V DC inlet voltage provides a nominal cooling flux of 6 [W] (online datasheet [23]). Here, thick bitumen samples were used (thickness ≈ 1 mm).

Optical and IR cameras were installed at a 30° angle with respect to the vertical, enabling simultaneous visualization (Figure S4b). The IR camera measurements allowed us to acquire the average surface temperature of an approximately 3 mm by 4.5 mm sample area.

2.5. Differential scanning calorimetry (DSC)

DSC experiments were performed using a PerkinElmer® 7, 1993 device. The DSC analysis was conducted using 11.75 ± 2.50 mg of both virgin and PCM-modified bitumen. In addition, experiments were conducted on the bitumen specimens with ~ 1 μl (1.22 ± 0.11 mg) of a single water droplet placed on top of a bitumen substrate in DSC sample molds under the same nitrogen purged environmental conditions of the DSC device (DSC baseline information when both sample holder were empty is provided in Figure S5 of Supporting Information, section "A.4.1".) We were interested in capturing material behavior at the cold temperature ranges with and without water. We performed the DSC measurements in a broader temperature range from 40 °C to −50 °C with two minutes of conditioning time at the limits of each thermal cycle. Three temperature cycles were performed in two 10 °C/min and 20 °C/min rates after initially heating samples to 40 °C from ambient temperature and conditioning for 2 min at 40 °C. (DSC analyses of virgin bitumen, PCM modified bitumen, and water [24] are reported in Figure S6a, b, and Figure S7, respectively, of Supporting Information, section "A.4.2".)

3. Results and discussion

Bitumen, as a pavement and sealing material, is always expected to be in direct contact with water. There are many manifestations of such interactions, but here we are interested in studying water droplets initially formed as condensate from a humid environment, which can subsequently freeze upon reduction of atmospheric temperature. Water condensation forms on cold surfaces below the dew point. Supercooled water droplet freezing is a complex phenomenon [25,26]. Upon cooling below its freezing point, condensed water is in a metastable, supercooled state, and in order to freeze, growing nuclei must overcome a free energy barrier to nucleation. Once overcome, further growth is energetically favorable, and such freezing is non-equilibrium and proceeds explosively fast (in the present study of the order of milliseconds) [26]. During this time, the droplets only partially solidify, as latent heat is released as ice grows [25,27]. Full solidification is completed in a subsequent markedly slower step (of the order of seconds; see Supporting Information, section "A.5.1" and Figure S8), which is governed by the balance of the released latent heat and heat removal [25,27].

Fig. 2 shows a micrograph and a temperature map of supercooled droplets condensed on bitumen. It can be seen that many droplets are still in a liquid state at temperatures far below 0 °C (surface temperature ~ -15 °C), while some droplets have frozen. Fig. 2a shows a droplet that has just started to freeze and is marked with a dotted circle. Fig. 2b shows an IR micrograph of a water droplet that has just started to freeze, and demonstrates that upon freezing—due to the rapidly released heat of fusion—the droplet actually attains a much higher temperature (the freezing equilibrium temperature of 0 °C) than its surroundings, which are still at −15 °C (Fig. 2b). Further implications of this heating phenomenon and its impact on droplet evaporation and freezing propagation will be discussed later in the paper.

Fig. 3 shows five selected timeframes of vapor condensation and freezing on virgin bitumen surfaces. Extracted synchronized frames from optical microscopy at temperature steps of 5 °C, −10 °C, −25 °C, −35 °C, and −50 °C at the −10 °C/min cooling rate

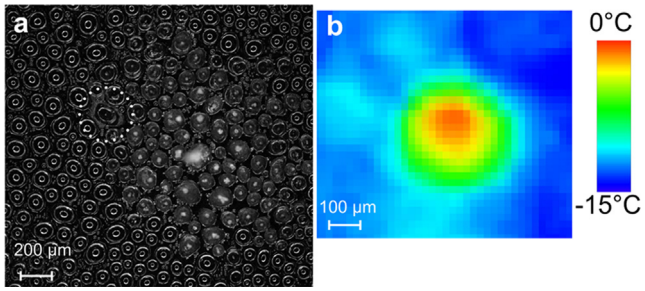

Fig. 2. Condensation freezing on the bitumen surface. a) optical image of the supercooled water droplets during freezing. The droplet in the white dotted circle is an example of a freezing water droplet. b) Infrared image of a freezing droplet. Due to the released latent heat of fusion at the moment of freezing, the temperature of a supercooled droplet jumps to the equilibrium water freezing temperature of 0 °C.

experiments, which started from 25 °C and proceeded until the target temperature of −50 °C was reached (see Video 1 in Supporting Information, section "B" for a full sequence of surface frosting). The continuous humidified nitrogen stream provided three relative humidity levels of 20%, 50%, and 80% (at T_{env} = 21.5 ± 0.5 °C), in Fig. 3a, Fig. 3b, and Fig. 3c, respectively. The ambient relative humidity changes the dew point; therefore, condensation is triggered at a warmer substrate temperature (earlier) in higher *RH* conditions for the same cooling rate (Fig. 3b, c). The size of the condensed droplets is larger under higher *RH* conditions (Fig. 3b and Fig. 3c) compared to low relative humidity conditions, such as a *RH* of 20% (Fig. 3a). The dotted area in the −35 °C temperature panels show the extent of the frozen areas in the field of view. We see that more frost grows faster for higher *RH* and the freezing temperature is also warmer, and denser frost forms at higher *RH* conditions after freezing (Fig. 3, -50 °C frame panels).

Fig. 4a and Fig. 4b show plots of condensation temperature vs. relative humidity (cooling rate = -10 °C /min) and condensation temperature vs. cooling rate (*RH* = 50%), respectively. Fig. 4c and Fig. 4d show plots of freezing temperature vs. relative humidity (cooling rate = -10 °C/min) and freezing temperature vs. cooling rate (*RH* = 50%), respectively. Fig. 4a shows that there is a correlation between relative humidity and condensation temperature. However, at the same RH, there is little correlation between cooling rate and condensation temperature, Fig. 4b. (We do observe that for different cooling rates, with constant *RH* = 50%, the final volume of the condensed droplets was larger at a slower cooling rate of −1 °C/min due to the longer residence time on the cold substrate in comparison to the faster cooling rate of −20 °C/min, Figure S9 and Supporting Information, section "A.5.2".) We see that as *RH* increases, for constant cooling rate, so too does the freezing temperature, Fig. 4c. We attribute this to the fact that under these conditions, more water can condense on the surface of bitumen when the relative humidity is higher, which increases the probability that a supercooled droplet will freeze. (Fig. 3c and Figure S9a show that for high relative humidity or low cooling rates, larger droplet-substrate contact diameters were observed just before freezing: ~600 to 1600 μm; Fig. 3a and Figure S9b-c show that for low relative humidity or intermediate or fast cooling rates, droplet-substrate contact diameters were ~ 50–60 μm, demonstrating the effects that cooling and relative humidity can have on condensed droplet sizes.) We also observe that the freezing temperature decreases with increased cooling rate, Fig. 4d. We attribute this to the fact that as the surface gets colder faster, it has less time to condense water on it—decreasing the overall volume of supercooled water on the surface—that in turn decreases the likelihood of freezing and therefore reduces the freezing temperature.

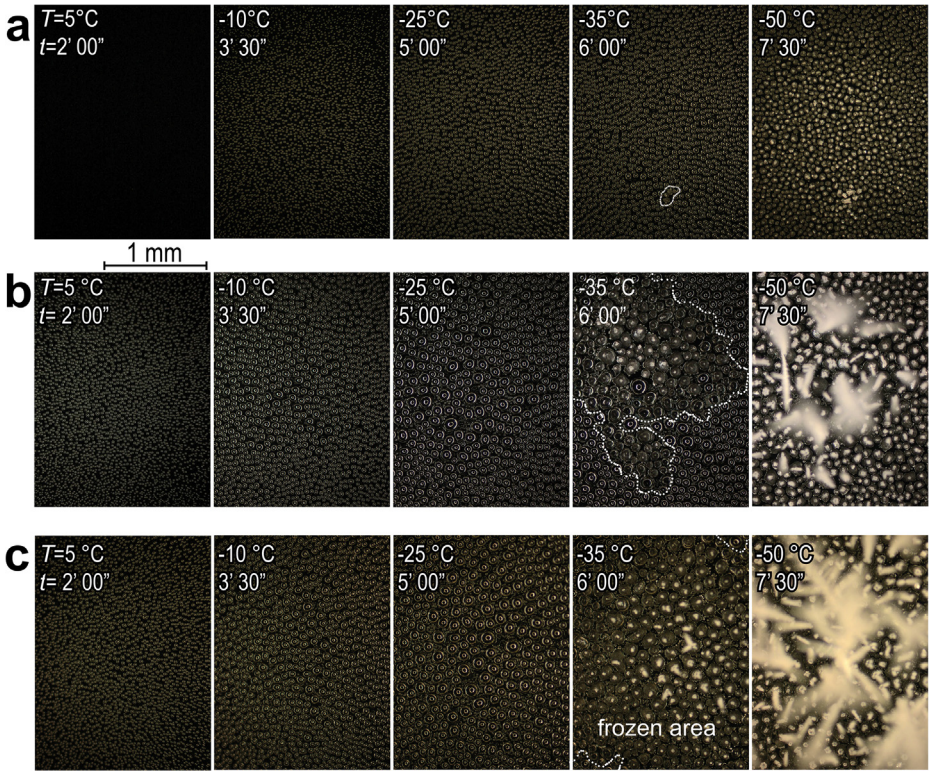

Fig. 3. Condensation and freezing on the surface of virgin bitumen under different environmental relative humidity (*RH*) conditions. Five temperature steps of 5 °C , −10 °C , −25 °C ,-35 °C , −50 °C (synchronized time steps) at −10 °C/min constant cooling rate under three different environmental *RH* conditions (T_{env} = 21.5 ± 0.5 °C) are shown. a) *RH* = 20% b) *RH* = 50% c) *RH* = 80%. Dotted regions at −35 °C panels show the extent of the frozen areas with different degrees of surface frosting: a, initiation (*RH* 20%), b, partially frozen (*RH* 50%), c, mostly frozen (*RH* 80%).

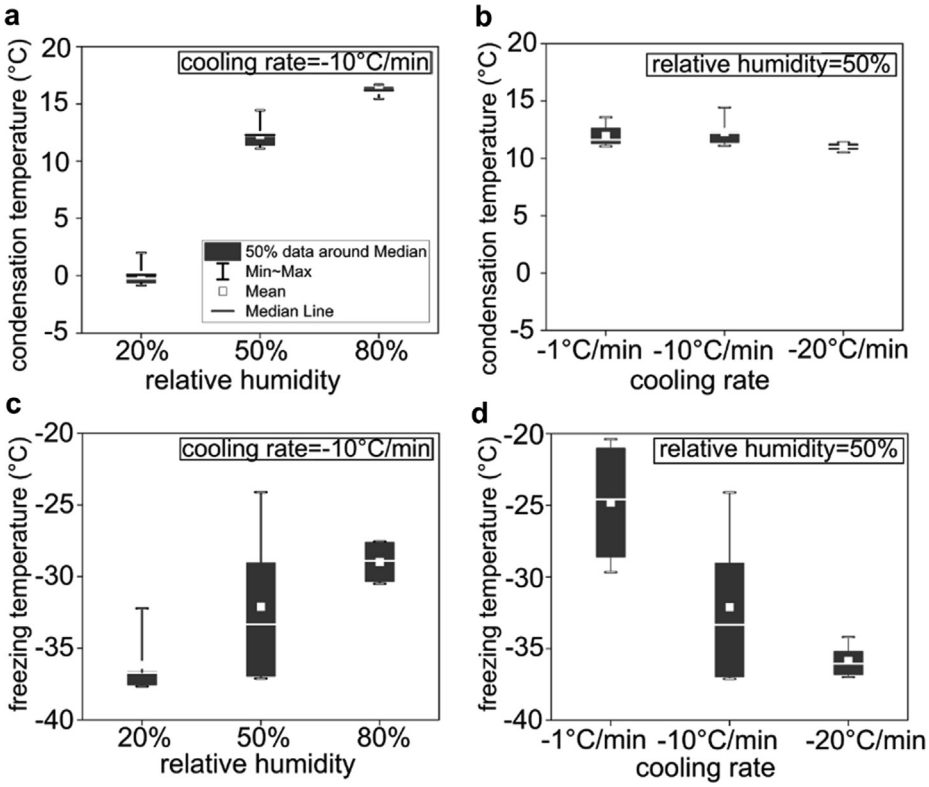

Fig. 4. Condensation and freezing on the surface of virgin bitumen under different conditions. Initial condensation temperature a) under three *RH* conditions of 20%, 50%, and 80% at −10 °C/min cooling rate. b) at three cooling rates −1 °C/min, −10 °C/min, and −20 °C/min at *RH* = 50%. Initial freezing temperature c) a) under three *RH* conditions of 20%, 50%, and 80% at −10 °C/min cooling rate. d) at three cooling rates −1 °C/min, −10 °C/min, and −20 °C/min at *RH* = 50%. (For all cases, T_{env} = 21.5 ± 0.5 °C).

Fig. 5a shows portions of three supercooled liquid droplets—one larger, two smaller—on the bitumen substrate, and Fig. 5b-d illustrates the very interesting phenomenon of "ice bridging", which manifests itself during freezing on the bituminous surface and is a mechanism facilitating frost spreading [27–30]. Previous work has shown that when a supercooled droplet freezes, it rapidly heats and evaporates, which here results in a condensation deposit, Fig. 5b [27]. Depending on the properties of the substrate, this deposit can freeze, forming a frost halo [27]. If there is a neighboring supercooled droplet, due to the high vapor pressure above it relative to the frozen droplet (for the same temperature), vapor diffusion can occur, resulting in an ice bridge forming between the frozen and supercooled droplets, Fig. 5c [28,29,31]. If the neighboring supercooled droplet is not too far away and is large enough to feed the growing ice bridge, then the ice bridge can form a connection between the two droplets and will cause the supercooled droplet to freeze [30] (see Video 2 in Supporting Information, section "B" which shows the full ice bridging process on bitumen).

To this end, we see that at subzero temperature conditions, suddenly, the large metastable droplet (Fig. 5a) suddenly freezes (Fig. 5b) with the mechanism discussed earlier. The simultaneously released latent heat is a practically adiabatic process (no heat losses within this very short time frame) [27]. This increases the droplet temperature to the equilibrium freezing temperature of 0 °C, making it significantly warmer than its environment and causing flash evaporation from the freezing droplet surface [25,27]. The so-generated excess vapor radially diffuses outward and subsequently condenses around the freezing droplet, forming a condensation deposit (Fig. 5b) [27]. The condensation occurs in the form of isolated supercooled micron-sized droplets, which are visible in the optical microscope results, Fig. 5b. Local vapor pressure gradients, substrate temperature, wettability, and substrate thermal conductivity govern the state of the condensation, whether or not this condensate deposit freezes, and desublimation around the frozen droplet [27] occurs. During the second slower stage of freezing (inner droplet freezing front propagation is not shown), whose rate is controlled by a balance of heat removal from the droplet into the substrate and latent heat of fusion, the droplet further solidifies. As a result of the droplet interface becoming ice and also eventually cooling, the evaporation rate also decreases [27]. Afterwards, in the vicinity of the freezing droplet, the local relative humidity gradually declines until it is locally in equilibrium with the ice. The vapor pressure above the ice is lower than that above supercooled water at the same temperature conditions. As a result, if there are supercooled droplets near the fully solidified droplet, the latter will act as a humidity sink to the former, causing evaporation. Hence, condensate droplets on the surface can evaporate and disappear altogether, Fig. 5c. Such vapor emitted from liquid evaporating/evaporated droplets can diffuse toward an adjacent ice droplet, deposit, and facilitate the formation and growth of an ice bridge, starting at the base of the larger frozen droplet, Fig. 5c. The ice bridge can act as freezing initiator for any neighboring supercooled liquid droplet that it can reach, Fig. 5d, leading to ice propagation and frost formation [29,30]. We see that the liquid droplet freezes as soon as the ice bridge connects, triggering the next iteration of bridging towards another liquid droplet, Fig. 5d.

Fig. 6a shows supercooled water droplets on bitumen before freezing (the dashed line shows the location of the cold pin). The latent heat that is released due to freezing raises the temperature of the supercooled droplets to their equilibrium freezing temperature, 0 °C (Fig. 6b-d). The evaporation rate of the droplet and the vapor pressure above it increases as a consequence. Eventually, the remaining surrounding supercooled droplets freeze. As discussed earlier, a plausible mechanism of the observed cascade freezing is ice bridging (Fig. 5). Additional mechanisms have also been discussed in literature [32]. Finally, the frozen area spreads, and frost covers the entire surface. (See also Figure S8 in Supporting Information, section "A.5.1" for a microscopic image sequence showing recalescence and freezing propagation and also the related Video 3 in section "B".)

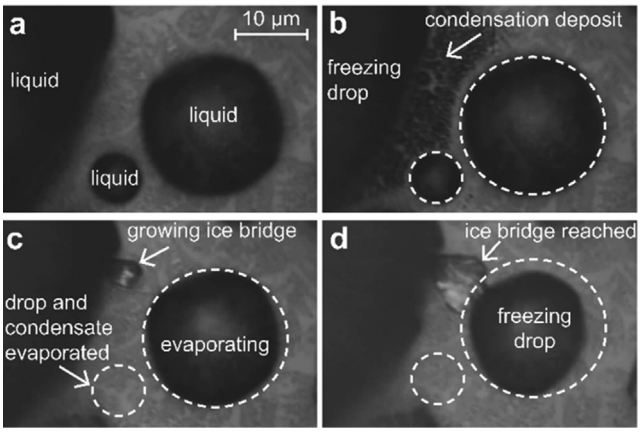

Fig. 5. Microscopic ice bridging and freezing propagation on bitumen. a) Three supercooled liquid droplets. b) Freezing of the large droplet forms condensation deposits. c) An ice bridge grows while the condensation deposit and the smallest liquid droplet evaporate. d) The ice bridge reaches the medium size drop and freezes it.

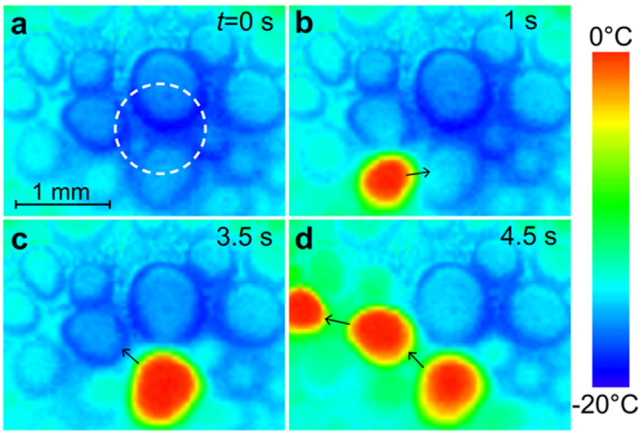

Fig. 6. Thermal imaging of recalescence and cascade freezing. a) Condensed supercooled water droplets on bitumen. The white dotted line shows the location of the cooling pin below the bituminous layer. b) Rapid release of latent heat of fusion during supercooled droplet freezing causes the droplet temperature to increase to the equilibrium value. c-d) Ice bridging or freezing of the condensate deposit, as discussed in Fig. 5, results in neighboring droplet freezing and "cascade freezing". Arrows show the direction of a cascading freezing event.

Based on the above, we have determined the environmental conditions under which condensed droplets form and freeze on bitumen. We now aim to use this knowledge and rationally select and embed a phase change material in bitumen and study supercooled droplet freezing behavior and how this could be affected by this modification. For this, we first studied the natural thermal properties of virgin bitumen in contact with water droplets, which is shown by the DSC measurements in Fig. 7a, b (see also Figure S6a, and Supporting Information, section "A.4.2"). Here we see that over this temperature range (-50 to 40 °C), the thermal properties of water dominate that of bitumen. (The exotherm and endotherm are attributed to supercooled water freezing and ice melting, respectively.) To alter the freezing behavior of water on bitumen, we opt to add PCM—with a melting temperature near the melting point of water—to bitumen in order to produce a heating effect,

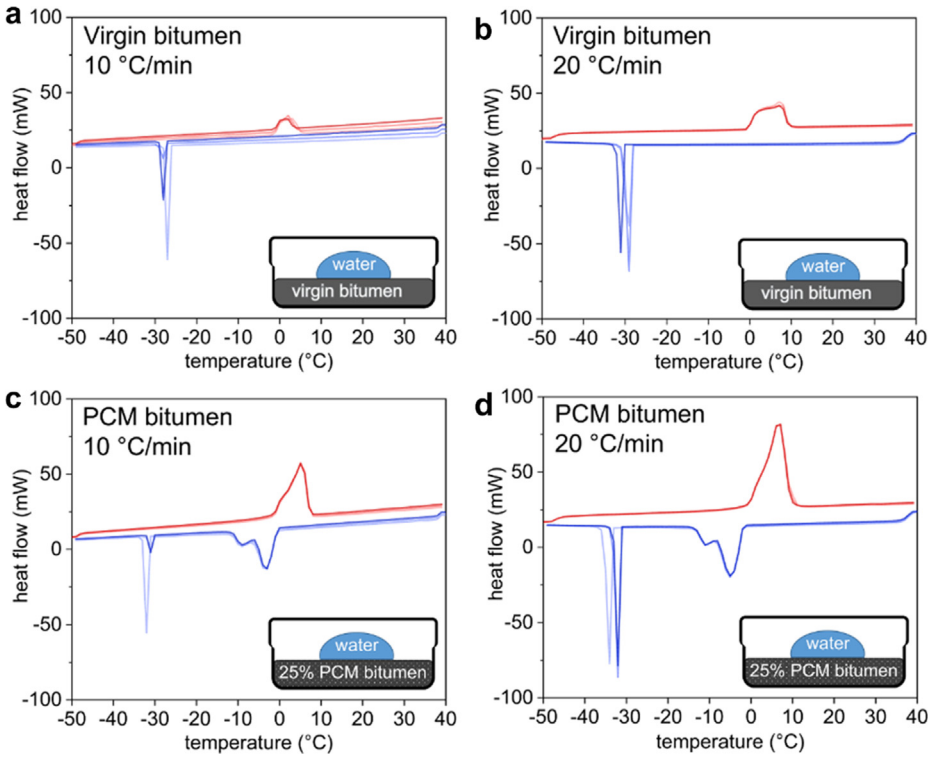

Fig. 7. DSC analysis of the virgin and modified bitumen when in contact with a 1 μl water droplet (positive heat flow indicates an endothermic process). a) Virgin bitumen at 10 °C/min rate, b) virgin bitumen at 20 °C/min rate, c) 25 wt% PCM modified bitumen at 10 °C/min rate, and d) 25 wt% PCM modified bitumen at 20 °C/min rate. Each plot has three heating and cooling cycles.

targeting the retardation of icing and aiding the significant heating effect from the latent heat of the water. Here we study the effect of embedded PCM microcapsules in virgin bitumen—at a concentration where it does not significantly alter the desirable mechanical properties of it (25 wt%) [15]—which we find can actively release heat over the temperature range of 1 °C to −20 °C, depending on the cooling rate (Fig. 7c, d, see also Figure S6b, and Supporting Information, section "A.4.2").

Despite the nature of metastable subcooled PCM material before crystallization, in the case of rapid PCM cooling (-20 °C/min), the crystallization activation of the PCM started at about the same temperature as the intermediate cooling (-10 °C/min), but the active temperature range—where the PCM still releases heat—depends on the time duration. Therefore, according to the cooling rates, the convoluted time durations on the temperature axis of the DSC results should be noted. (The measured PCM fusion peak temperature values are in the range of the −4 ± 3 °C; see Supporting Information "A″, Figure S6b and Fig. 7.) Kakar et al. [15] showed for the same PCM microencapsulated modified bitumen that we used here, the cold temperature mechanical performance of the material was improved by embedding 25 wt% PCM in bitumen. Moreover, it has also been shown that this PCM microcapsule remains stable in the bitumen mixture without agglomeration [15]. The DSC analysis detected water freezing latent heat release of 17 ± 9 J/g on both modified and virgin bitumen, while the PCM heat of fusion at 25 wt% concentration is 48 ± 3 J/g, Fig. 7c, d. It is noted that the freezing temperature of a 1 μl water droplet on PCM modified bitumen is up to ~ 7 °C lower compared to a water droplet freezing on control virgin bitumen specimens. We attribute this difference to the fact that the PCM releases a significant amount of heat, warming the droplet, meaning that the system is not isothermal and has to cool itself more in order to trigger supercooled droplet freezing.

Fig. 8a, b show the difference in frost development after 3 min of constant flux cooling on the virgin bitumen and the PCM-modified bitumen, respectively. Different degrees of frost formation and condensation indicate that there are differences in substrate temperature at the same environmental conditions. Analyzing the optical and infrared results of both surfaces shows that condensed water requires almost twice as long to freeze on the PCM-bitumen composite compared to the virgin bitumen at the same cooling and environmental conditions (Fig. 8c). This means that the latent heat of fusion from the PCM microcapsules can delay the freezing of water on the bitumen surface. IR surface temperature measurements reveal that the bitumen containing PCM cools at a slower rate and has a significant effect on the surface temperature of bitumen, Fig. 8d. PCM activation occurs gradually as the cooling is done from the bottom of the bitumen, manifesting itself as a kink in the temperature profile of the surface temperature once the PCM effect reaches the surface. The IR surface temperature history plots show that eventually, even after releasing all stored PCM heat, the surface temperature of modified bitumen remained at least 10 °C warmer at similar time steps compared to control virgin bitumen sample temperature at −30 °C, Fig. 8d. We also see that the modified bitumen surface remains warmer even after freezing has initiated, which has implications for subsequent ice removal, as ice is known to adhere stronger to substrates at colder temperatures compared to warmer ones [33]. We note that in many applications, the surface of bitumen may be contaminated—affecting and possibly promoting condensation nucleation and freezing—and that the present approach, which is based on embedding PCMs to enhance surface heating and nucleation delay should also work to delay freezing under such challenging real-world conditions since it is based upon the bulk modification of bitumen and not the surface alone.

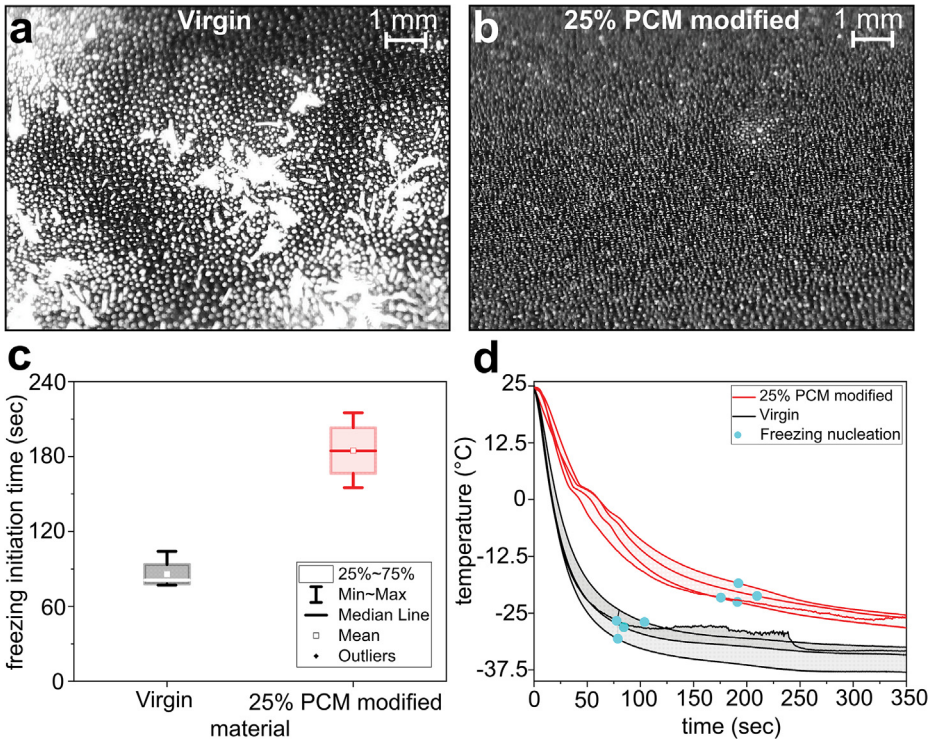

Fig. 8. PCM can delay freezing on bitumen. Bitumen surfaces after 3 min cooling at the same constant cooling flux condition from 25 °C for two material states of a) Virgin. b) 25 wt% PCM-modified bitumen. c) Freezing initiation time on a bitumen surface plotted for virgin and 25 wt% PCM-modified bitumen in black and red colors, respectively. d) Bitumen surface temperature measured by IR camera plotted for virgin and 25 wt% PCM-modified bitumen in black and red colors, respectively. PCM activation occurs gradually as the cooling is done from the bottom of the bitumen. This manifests itself into a kink in the temperature profile of the surface temperature once the PCM effect reaches the surface. Initial freezing nucleation temperatures are marked with blue circle symbols. (For interpretation of the references to colour in this figure legend, the reader is referred to the web version of this article.)

4. Conclusion

The complex process of condensation and freezing of water on bituminous materials was investigated. It was found that the initial temperature at which condensation initiated is highly dependent on the relative humidity and the available vapor above the cold surface. Different substrate cooling rates have a minor effect on the initial condensation temperature. However, for slow cooling rates, where bitumen remains exposed to colder temperatures for a longer period of time, water upon it freezes at relatively higher subzero temperatures. At the moment of freezing, the released latent heat causes the temperature of the supercooled droplets to jump to 0 °C, the equilibrium freezing temperature, causing local heating and evaporation. Subsequent local condensation of this vapor and its freezing among droplets initiates an interesting phenomenon of ice bridging and frost propagation, which we reveal with optical microscopy and high-speed infrared imaging. Embedding PCM microcapsules with a melting temperature close to that of water and at 25 wt% in bitumen—a concentration that does not significantly alter mechanical properties—can markedly delay supercooled water freezing and frost formation. It is experimentally shown in the designed experimental condition and 25 wt% concentration of the PCM microcapsules in bitumen, that the average freezing time shifts from about 85 s on virgin bitumen to about 185 s on PCM modified bitumen. This effect can postpone freezing incidence in constant heat flux cooling and maintain ice-free bitumen surfaces. As discussed earlier, previous research has shown that the microcapsules can stay intact during the fabrication of asphalt concrete, as long as this is the case, the effect of PCM's is repeated through the melting and crystallization cycle dictated by the natural temperature fluctuations. Future research could focus on in situ performance of such novel additives.

CRediT authorship contribution statement

F. Tarpoudi Baheri: Investigation, Methodology, Formal analysis, Validation, Visualization, Writing - original draft. **L.D. Poulikakos:** Conceptualization, Supervision, Writing - original draft, Funding acquisition. **D. Poulikakos:** Conceptualization, Writing - original draft. **T.M. Schutzius:** Conceptualization, Supervision, Writing - original draft.

Declaration of Competing Interest

The authors declare that they have no known competing financial interests or personal relationships that could have appeared to influence the work reported in this paper.

Acknowledgments

Financial support of the Swiss National Science Foundation under grant number 200020_169122 / 1 and the European Research Council under Advanced Grant 669908 (INTICE) are acknowledged. Beatrice Fischer of Empa is acknowledged for performing the DSC measurements.

Appendix A. Supplementary data

Supplementary data to this article can be found online at https://doi.org/10.1016/j.conbuildmat.2021.123851.

References

[1] Read, J.; Whiteoak, D. The Shell Bitumen Handbook, 5th Edition, 5th ed.; Thomas Telford Ltd: London, 2003. 10.1680/sbh.32200.

[2] Y. Yao, X. Zhao, Y. Zhang, C. Chen, J. Rong, Modeling of Individual Vehicle Safety and Fuel Consumption under Comprehensive External Conditions, Transp. Res. Part D Transp. Environ. 79 (January) (2020), https://doi.org/10.1016/j.trd.2020.102224 102224.
[3] D.L. Kelting, C.L. Laxson, Review of Effects and Costs of Road De-Icing with Recommendations for Winter Road Management in the Adirondack Park, New York, NY, Adirondack Watershed Institute, 2010.
[4] F. Malin, I. Norros, S. Innamaa, Accident Risk of Road and Weather Conditions on Different Road Types, Accid. Anal. Prev. 2019 (122) (February 2018) 181–188, https://doi.org/10.1016/j.aap.2018.10.014.
[5] T. Usman, L. Fu, L.F. Miranda-Moreno, Quantifying Safety Benefit of Winter Road Maintenance: Accident Frequency Modeling, Accid. Anal. Prev. 42 (6) (2010) 1878–1887, https://doi.org/10.1016/j.aap.2010.05.008.
[6] J. Norrman, M. Eriksson, S. Lindqvist, Relationships between Road Slipperiness, Traffic Accident Risk and Winter Road Maintenance Activity, Clim. Res. 15 (3) (2000) 185–193, https://doi.org/10.3354/cr015185.
[7] A.K. Andersson, L. Chapman, The Impact of Climate Change on Winter Road Maintenance and Traffic Accidents in West Midlands, UK. *Accid. Anal. Prev.* 43 (1) (2011) 284–289, https://doi.org/10.1016/j.aap.2010.08.025.
[8] I. Juga, P. Nurmi, M. Hippi, Statistical Modelling of Wintertime Road Surface Friction, Meteorol. Appl. 20 (3) (2013) 318–329, https://doi.org/10.1002/met.1285.
[9] F. Giuliani, F. Merusi, G. Polacco, S. Filippi, M. Paci, Effectiveness of Sodium Chloride-Based Anti-Icing Filler in Asphalt Mixtures, Constr. Build. Mater. 30 (2012) 174–179, https://doi.org/10.1016/j.conbuildmat.2011.12.036.
[10] F. Autelitano, M. Rinaldi, F. Giuliani, Winter Highway Maintenance Strategies: Are All the Sodium Chloride Salts the Same?, Constr. Build. Mater. 226 (2019) 945–952, https://doi.org/10.1016/j.conbuildmat.2019.07.292.
[11] Y. Hassan, A.O. Abd El Halim, A.G. Razaqpur, W. Bekheet, M.H. Farha, Effects of Runway Deicers on Pavement Materials and Mixes: Comparison with Road Salt, J. Transp. Eng. 128 (4) (2002) 385–391, https://doi.org/10.1061/(ASCE)0733-947X(2002)128:4(385).
[12] X. Shi, M. Akin, T. Pan, L. Fay, Y. Liu, Z. Yang, Deicer Impacts on Pavement Materials: Introduction and Recent Developments, Open Civ. Eng. J. 3 (1) (2009) 16–27, https://doi.org/10.2174/1874149500903010016.
[13] J.H. Judd, Lake Stratification Caused by Runoff from Street Deicing, Water Res. 4 (8) (1970) 521–532, https://doi.org/10.1016/0043-1354(70)90002-3.
[14] Z. Refaa, M.R. Kakar, A. Stamatiou, J. Worlitschek, M.N. Partl, M. Bueno, Numerical Study on the Effect of Phase Change Materials on Heat Transfer in Asphalt Concrete, Int. J. Therm. Sci. 133 (March) (2018) 140–150, https://doi.org/10.1016/j.ijthermalsci.2018.07.014.
[15] M.R. Kakar, Z. Refaa, J. Worlitschek, A. Stamatiou, M.N. Partl, M. Bueno, Effects of Aging on Asphalt Binders Modified with Microencapsulated Phase Change Material, Compos. Part B Eng. 173 (June) (2019), https://doi.org/10.1016/j.compositesb.2019.107007 107007.
[16] H.R. Fischer, E.C. Dillingh, C.G.M. Hermse, On the Microstructure of Bituminous Binders, Road Mater. Pavement Des. 15 (1) (2014) 1–15, https://doi.org/10.1080/14680629.2013.837838.
[17] H. Soenen, J. Besamusca, H.R. Fischer, L.D. Poulikakos, J.-P. Planche, P.K. Das, N. Kringos, J.R.A. Grenfell, X. Lu, E. Chailleux, Laboratory Investigation of Bitumen Based on Round Robin DSC and AFM Tests, Mater. Struct. 47 (7) (2014) 1205–1220, https://doi.org/10.1617/s11527-013-0123-4.
[18] M.R. Kakar, Z. Refaa, M. Bueno, J. Worlitschek, A. Stamatiou, M.N. Partl, Investigating Bitumen's Direct Interaction with Tetradecane as Potential Phase Change Material for Low Temperature Applications, Road Mater. Pavement Des. 21 (8) (2020) 2356–2363, https://doi.org/10.1080/14680629.2019.1601127.
[19] M.R. Kakar, Z. Refaa, J. Worlitschek, A. Stamatiou, M.N. Partl, M. Bueno, Thermal and Rheological Characterization of Bitumen Modified with Microencapsulated Phase Change Materials, Constr. Build. Mater. 215 (2019) 171–179, https://doi.org/10.1016/j.conbuildmat.2019.04.171.
[20] M. Bueno, M.R. Kakar, Z. Refaa, J. Worlitschek, A. Stamatiou, M.N. Partl, Modification of Asphalt Mixtures for Cold Regions Using Microencapsulated Phase Change Materials, Sci. Rep. 9 (1) (2019), https://doi.org/10.1038/s41598-019-56808-x 20342.
[21] G. Vali, Interpretation of Freezing Nucleation Experiments: Singular and Stochastic, Sites and Surfaces. *Atmos. Chem. Phys.* 14 (11) (2014) 5271–5294, https://doi.org/10.5194/acp-14-5271-2014.
[22] R.O. Suzuki, T. Fujisaka, K.O. Ito, X. Meng, H.T. Sui, Dimensional Analysis of Thermoelectric Modules Under Constant Heat Flux, J. Electron. Mater. 44 (1) (2015) 348–355, https://doi.org/10.1007/s11664-014-3314-z.
[23] Laird Thermal Systems https://www.lairdthermal.com/products/thermoelectric-cooler-modules/peltier-thermal-cycling-series/PC6-12-F1-4040-TA-W6 (accessed Nov 12, 2020).
[24] D.R. Legates, in: Encyclopedia of Earth Sciences SeriesEncyclopedia of World Climatology, Springer Netherlands, 2005, pp. 450–451, https://doi.org/10.1007/1-4020-3266-8_124.
[25] G. Graeber, T.M. Schutzius, H. Eghlidi, D. Poulikakos, Spontaneous Self-Dislodging of Freezing Water Droplets and the Role of Wettability, Proc. Natl. Acad. Sci. 114 (42) (2017) 11040–11045, https://doi.org/10.1073/pnas.1705952114.
[26] S. Jung, M.K. Tiwari, N.V. Doan, D. Poulikakos, Mechanism of Supercooled Droplet Freezing on Surfaces, Nat. Commun. 3 (1) (2012) 615, https://doi.org/10.1038/ncomms1630.
[27] S. Jung, M.K. Tiwari, D. Poulikakos, Frost Halos from Supercooled Water Droplets, Proc. Natl. Acad. Sci. U. S. A. 109 (40) (2012) 16073–16078, https://doi.org/10.1073/pnas.1206121109.
[28] S. Nath, S.F. Ahmadi, J.B. Boreyko, A Review of Condensation Frosting, Nanoscale Microscale Thermophys. Eng. 21 (2) (2017) 81–101, https://doi.org/10.1080/15567265.2016.1256007.
[29] S. Nath, J.B. Boreyko, On Localized Vapor Pressure Gradients Governing Condensation and Frost Phenomena, Langmuir 32 (33) (2016) 8350–8365, https://doi.org/10.1021/acs.langmuir.6b0148810.1021/acs.langmuir.6b01488.s001.
[30] S. Nath, S.F. Ahmadi, J.B. Boreyko, How Ice Bridges the Gap, Soft Matter 16 (5) (2020) 1156–1161, https://doi.org/10.1039/c9sm01968e.
[31] J.B. Boreyko, C.P. Collier, Delayed Frost Growth on Jumping-Drop Superhydrophobic Surfaces, ACS Nano 7 (2) (2013) 1618–1627, https://doi.org/10.1021/nn3055048.
[32] G. Graeber, V. Dolder, T.M. Schutzius, D. Poulikakos, Cascade Freezing of Supercooled Water Droplet Collectives, ACS Nano 12 (11) (2018) 11274–11281, https://doi.org/10.1021/acsnano.8b05921.
[33] T. Chen, Q. Cong, C. Sun, J. Jin, K.L. Choy, Influence of Substrate Initial Temperature on Adhesion Strength of Ice on Aluminum Alloy, Cold Reg. Sci. Technol. 148 (January) (2018) 142–147, https://doi.org/10.1016/j.coldregions.2018.01.017.